Triple Combination of MEK, BET, and CDK Inhibitors Significantly Reduces Human Malignant Peripheral Nerve Sheath Tumors in Mouse Models

Sara Ortega-Bertran[1,2,3], Juana Fernández-Rodríguez[1,2,4,5], Miriam Magallón-Lorenz[6], Xiaohu Zhang[7], Edgar Creus-Bachiller[1,2], Adriana Paola Diazgranados[8], Itziar Uriarte-Arrazola[6], Helena Mazuelas[6], Ignacio Blanco[9], Claudia Valverde[10,11], Meritxell Carrió[6], Alberto Villanueva[2,12], Thomas De Raedt[13,14], Cleofé Romagosa[8,4], Bernat Gel[6,15], Héctor Salvador[16], Marc Ferrer[7], Conxi Lázaro[1,2,4], and Eduard Serra[6,4]

ABSTRACT

Purpose: Malignant peripheral nerve sheath tumor (MPNST) is an aggressive soft-tissue sarcoma that develops sporadically or in patients with neurofibromatosis type 1 (NF1). Its development is marked by the inactivation of specific tumor suppressor genes (TSG): *NF1*, *CDKN2A*, and *SUZ12*/*EED* (polycomb repressor complex 2). Each TSG loss can be targeted by particular drug inhibitors, and we aimed to systematically combine these inhibitors, guided by TSG inactivation status, to test their precision medicine potential for MPNSTs.

Experimental Design: We performed a high-throughput screening in 3 MPNST cell lines testing 14 MEK inhibitors (MEKi), 11 cyclin-dependent kinase 4/6 inhibitors (CDKi), and 3 bromodomain inhibitors (BETi) as single agents and 147 pairwise co-treatments. Best combinations were validated in nine MPNST cell lines, and three were tested in one sporadic and one NF1-associated patient-derived orthotopic xenograft (PDOX) MPNST mouse model. A final combination of the three inhibitor classes was tested in the same PDOX models.

Results: A high degree of redundancy was observed in the effect of compounds of the same inhibitory class, individually or in combination, and responses matched with TSG inactivation status. The MEKi–BETi (ARRY-162 + I-BET151) co-treatment triggered a reduction in half of the NF1-related MPNST PDOXs and all the sporadic tumors, reaching 65% reduction in tumor volume in the latter. Remarkably, this reduction was further increased in both models combining the three inhibitor classes, reaching 85% shrinkage on average in the sporadic MPNST.

Conclusions: Our results strongly support precision therapies for MPNSTs guided by TSG inactivation status. MEKi–BETi CDKi triple treatment elicits a significant reduction of human MPNST PDOXs.

Introduction

Malignant peripheral nerve sheath tumor (MPNST) is an aggressive soft-tissue sarcoma occurring in three distinct clinical settings: associated with neurofibromatosis type 1 (NF1; 40%–50%), in sporadic cases (40%–47%), and at sites of previous radiotherapy (10%–13%; ref. 1). The lifetime risk of an individual with NF1 of developing an MPNST is about 10%, being the leading cause of mortality in this genetic disease (2–4). MPNSTs have a poor prognosis because of its invasive growth and propensity to metastasize (5). These tumors are usually high-grade malignant spindle-cell neoplasms arising in association with large peripheral nerves (6). MPNST diagnosis is challenging because of the lack of distinctive molecular markers and the overlapping histologic presentations with other tumor entities (7).

The primary treatment for a localized MPNST is complete surgical excision with wide negative margins, followed by radiotherapy and/or chemotherapy. However, this procedure is often

[1]Hereditary Cancer Program, Catalan Institute of Oncology (ICO-IDIBELL), Hospitalet de Llobregat, Barcelona, Spain. [2]Program in Molecular Mechanisms and Experimental Therapy in Oncology (Oncobell), IDIBELL, Hospitalet de Llobregat, Barcelona, Spain. [3]Doctoral Program in Biomedicine, University of Barcelona, Barcelona, Spain. [4]Centro de Investigación Biomédica en Red de Cáncer (CIBERONC), Madrid, Spain. [5]Mouse Lab, SCT-IDIBELL, Hospitalet de Llobregat, Barcelona, Spain. [6]Hereditary Cancer Group, CARE Translational Program, Germans Trias i Pujol Research Institute (IGTP), Badalona, Barcelona, Spain. [7]Division of Preclinical Innovation, National Center for Advancing Translational Sciences, NIH, Rockville, Maryland. [8]Pathology Department, Hospital Universitari Vall d'Hebron and Vall d'Hebron Research Institute (VHIR), Barcelona, Spain. [9]Clinical Genetics Department, Laboratori Clínic de la Metropolitana Nord, Hospital Universitari Germans Trias i Pujol, Badalona, Barcelona, Spain. [10]Department of Medical Oncology, Hospital Universitari Vall d'Hebron, Barcelona, Spain. [11]Vall d'Hebron Institute of Oncology, Barcelona, Spain. [12]Procure Program, Catalan Institute of Oncology, Hospitalet de Llobregat, Barcelona, Spain. [13]Department of Pediatrics, Children's Hospital Philadelphia, Philadelphia, Pennsylvania. [14]School of Medicine, University of Pennsylvania, Philadelphia, Pennsylvania. [15]Departament de Fonaments Clínics, Facultat de Medicina i Ciències de la Salut, Universitat de Barcelona (UB), Barcelona, Spain. [16]Pediatric Oncology Department, Sant Joan de Déu Barcelona Children's Hospital, Barcelona, Spain.

C. Lázaro and E. Serra contributed equally to this article.

Corresponding Author: Eduard Serra, Germans Trias i Pujol Research Institute (IGTP), Carretera de Can Ruti, Camí de les Escoles s/n, Badalona, Barcelona 08916, Spain. E-mail: eserra@igtp.cat

Clin Cancer Res 2025;31:907–20

doi: 10.1158/1078-0432.CCR-24-2807

Translational Relevance

Malignant peripheral nerve sheath tumor (MPNST) is a very aggressive soft-tissue sarcoma of the peripheral nervous system with a poor prognosis. Most treatments reported to date using human MPNST patient-derived xenografts have been able to reduce the rate of tumor growth compared with controls. We report here the first systematic attempt to inform on the possibilities of using precision medicine for MPNSTs guided by the inactivation status of the three most recurrently lost tumor suppressor genes in this tumor type. In fact, we have identified that the MEK inhibitor–bromodomain inhibitor–cyclin-dependent kinase inhibitor triple treatment consistently reduces tumor size in two human MPNST patient-derived orthotopic xenograft models, one sporadic and one neurofibromatosis type 1–associated. This represents a novel and promising combination for the treatment of MPNSTs. These preclinical data on human MPNSTs are very valuable to inform current and future clinical trials for MPNSTs.

compromised by tumor infiltration, location, or size, resulting in a high relapse rate. Currently, there is no effective treatment for patients with metastatic disease (8, 9). There is a clear need to identify effective treatments for MPNSTs. To this end, the development of faithful *in vitro* and *in vivo* preclinical models is key to discover new therapies. Currently, different human MPNST-derived models exist, like a large set of MPNST cell lines and different types of patient-derived xenografts (PDX) mouse models (10). Orthotopically engrafted PDX reliably recapitulate the histology and genomics of human primary tumors and can reproduce their metastatic capacity (11, 12).

MPNSTs are characterized by a low frequency of small mutations and highly rearranged and hyperploid genomes (13). Their initial development is marked by the inactivation of three tumor suppressor genes (TSG): *NF1*, *CDKN2A*, and *SUZ12* or *EED* (polycomb repressive complex 2, PRC2) in both sporadic and NF1-associated MPNSTs (14, 15). The *NF1* gene codes for neurofibromin, which negatively regulates the Ras/MAPK pathway, involved in cell proliferation (16). MEK inhibitors (MEKi) are used to counteract pathway overactivation caused by the *NF1* loss (17). The *CDKN2A* locus codes for two proteins ($p16^{INK4a}$ and $p14^{ARF}$). $p16^{INK4a}$ prevents the formation of the cyclin-dependent kinase (CDK)4/cyclin D1 complex, regulating the retinoblastoma protein (RB) and resulting in cell-cycle arrest. $p14^{ARF}$ binds to Mdm2 to release and regulate p53 degradation. Loss of *CDKN2A* may compromise senescence, facilitating malignant transformation (18). On this basis, CDK inhibitors (CDKi) may compensate *CDKN2A* loss in MPNSTs (19). The PRC2 complex is a crucial epigenetic regulator of cellular homeostasis that maintains transcriptionally silent chromatin through the trimethylation of histone H3 at lysine 27 (H3K27me3). In MPNST, loss of *SUZ12* or *EED* triggers an epigenetic change, leading to increased global levels of H3K27 acetylation, recruiting members of the bromodomain and extraterminal domain (BET) family of epigenetic reader proteins, such as BRD4, and regulating the transcription of genes such as c-*MYC*, *TP53*, or members of the Ras pathway, thereby amplifying cell proliferation (20). BET inhibitors (BETi) can competitively bind to bromodomains altering gene expression regulation (20, 21).

Therefore, the use of these three types of inhibitors (MEKi, CDKi, and BETi), especially in combination, may be a good therapeutic strategy for MPNSTs. Previous studies tested these inhibitors in MPNST models *in vitro* and *in vivo* as single agents, achieving cytostatic effects in tumor growth (17, 20–22), or in combination with other compounds, providing superior treatment responses (19, 20). High-throughput screening (HTS) platforms enable the analysis of single and combinations of drugs at a large scale (23). In this study, all MEKi, CDKi, and BETi of the Mechanism Interrogation PlatE (MIPE) 4.0 oncology library of the National Center for Advancing Translational Sciences (NCATS) were tested in a systematic manner, as single agents and selected pairwise combinations. This analysis provides a conclusive view of the therapeutic potential of a precision medicine strategy for MPNST based on the inactivation status of *NF1*, *CDKN2A*, and PRC2. Promising combinations were validated in a large panel of nine MPNST cell lines. Three best combinations were tested *in vivo* in two independent human MPNST orthotopic PDXs (PDOX), one NF1-related, and one sporadic.

Materials and Methods

Cell lines

Four MPNST cell lines (NF1-08, NF1-09, NF1-18B, and SP-10) were established in our lab (data not shown; ref. 12), whereas five were obtained from other labs: S462 (RRID: CVCL_1Y70; ref. 24), sNF96.2 (RRID: CVCL_K281; ref. 25), ST88-14 (RRID: CVCL_8916; ref. 26), NF90-8 (RRID: CVCL_1B47; ref. 27), and NMS-2 (RRID: CVCL_4662; refs. 15, 28). The human foreskin fibroblast (HFF-1) cell line (Banco de Células do Rio de Janeiro Cat. #0275, RRID: CVCL_3285) from ATCC (SCRC-1041) was also used. Cells were maintained in DMEM + GlutaMAX with 10% FBS and 1% penicillin and streptomycin at 37°C with 5% CO_2. All cell lines were tested for *Mycoplasma* before experimental procedures.

Quantitative HTS

Drugs from the NCATS MIPE 4.0 library targeting MEK, CDK, or BRD4 (BET) were screened in S462, NF1-08, and NF1-09 cell lines. Briefly, compounds were tested in an 11-point dose-response (starting at a stock concentration of 10 mmol/L, until the maximum concentration of 46 μmol/L), and cell viability was measured using CellTiter-Glo (CTG) after 48 hours (29). Viability was normalized to DMSO-treated controls. The activity of the compounds was determined based on their curve response class (CRC; Supplementary Fig. S1; ref. 30). Combination screening followed previous protocols (31). Data from the 147 10 × 10 combination screening matrices are provided in Supplementary Table S1.

In vitro validation of combinations

All compounds were provided by the NCATS Compound Management group in DMSO solutions at 10 mmol/L. The IC_{50} of each compound was calculated in nine MPNST cell lines (Supplementary Table S2). Between 5,000 and 12,000 cells/well were seeded in 96-well plates and incubated overnight. Compounds were added in triplicates at five concentrations. After 48 hours, cell viability was assessed using the 3-[4,5-dimethylthiazol-2-yl]-2,5 diphenyl tetrazolium bromide assay (Sigma-Aldrich), and the absorbance was measured in a Victor X5 2030 Multilabel Reader (PerkinElmer). For the combination assays, we used the same protocol for single compounds but at a fixed 1:1 ratio of the IC_{50} for each compound. Synergy was determined using

CompuSyn software (RRID: SCR_022931), based on Chou–Talalay calculations (32).

Maximum tolerated dose test

Maximum tolerated doses (MTD) and drug administration were tested on 6-week-old male athymic nude mice (athymic nude-*Foxn1*^{nu}, Envigo, RRID: IMSR_CRL:490) without tumors. Mice were treated with compounds for 3 weeks, with daily weight measurements to assess toxicity. Drugs were purchased from MedChemExpress: ARRY-162 (binimetinib, Cat. # HY-1520), I-BET151 (Cat. #HY-13235), and ribociclib (Cat. #HY-15777). No toxicity was observed at any dose. The MTD values and guidelines for the administration of compounds are provided in Supplementary Fig. S2.

In vivo drug testing on MPNST PDOX models

SP-10 and NF1-18B PDOX models were established in our lab (data not shown). Tumors were expanded in 5-week-old athymic nude mice. When tumors reached 1,000 to 1,500 mm^3, they were grafted into the sciatic nerve of new 5-week-old mice. Each group consisted of 5 to 10 mice. Once tumors reached 300 to 500 mm^3, mice were randomized into treatment groups and treated for 2 weeks (ARRY-162 15 mg/kg, orally, twice daily; I-BET151 30 mg/kg i.p., daily; ribociclib 90 mg/kg, orally, daily). Mice were sacrificed 4 to 5 hours after the last dose, and tumors were removed. Tumors were measured using a caliper twice a week, and the volume was calculated using the formula $v = (w^2\ L/2)$, in which L is the longest diameter and w is the width. For tumor regrowth, the protocol included 3 weeks of treatment, 2 weeks of resting, and another 3 weeks of treatment. For triple treatments, the protocol included 3 weeks of treatment and a different dosage for ribociclib (85 mg/kg, orally, daily). Statistical analyses used the Mann–Whitney test, with a significance level at 0.05.

Protein extraction and Western blot analysis

Protein was extracted from 15 to 20 mg of tumor homogenized in RIPA buffer with protease inhibitor using TissueLyser II (RRID: SCR_018623) and centrifuged at 16,000 × *g* at 4°C for 10 minutes. Cell pellets were resuspended in RIPA buffer, incubated at 95°C for 20 minutes, and centrifuged. Protein was quantified with the Pierce BCA Protein Assay Kit (Thermo Fisher Scientific). For Western blotting, 20 μg of protein was separated on 12% SDS-acrylamide gels (Bio-Rad) and transferred to nitrocellulose membranes. Membranes were blocked with BSA and incubated with primary antibodies (Supplementary Table S3A) overnight at 4°C. Detection used SuperSignal West Femto chemiluminescent substrate kits (Thermo Fisher Scientific). Quantification was done using Image Lab, normalizing proteins to tubulin, vinculin, or GAPDH.

RNA extraction and RT-qPCR analysis

Between 80,000 and 140,000 cells of six cell lines (S462, NF1-18B, SP-10, STS-26T, Sch-2, and NF1-09) were seeded in six-well plates and incubated overnight. Cells were either untreated, treated with I-BET151, or treated with ARRY-162 + I-BET151 (1:1 IC_{50} ratio) for NF1-18B and SP-10. After 20 hours, cells were scraped and RNA isolated using TRI Reagent and ethanol. Total RNA was extracted with the Direct-zol RNA MiniPrep kit (Zymo Research) and quantified using a NanoDrop 1000 (RRID: SCR_016517) spectrophotometer. RNA (0.5 μg) was reverse-transcribed using SuperScript III (Life Technologies). RT-qPCR was performed with LightCycler 480 SYBR Green I Master (Roche) and analyzed using the LightCycler 480 real-time PCR system (Roche). Gene expression was normalized to *EP300* and *TBP* and expressed as normalized relative expression. Primer sequences are provided in Supplementary Table S3B. Data analysis and representation were performed using Microsoft Excel and GraphPad Prism (version 7.03; RRID: SCR_002798).

RNA sequencing

The RNA sequencing (RNA-seq) library was prepared at BGI using DNBSEQ standard protocols. Data were aligned using Salmon v1.8.0 (RRID: SCR_017036; ref. 33) against the UCSC refMrna and hg38 genome. Transcript-level estimates were imported into R (R v4.3.0 Bioconductor v3.17) and summarized to the gene level using tximport (RRID: SCR_016752; ref. 34). Genes with less than five counts in more than two samples were filtered out. A principal component analysis (PCA) plot was generated. Differentially expressed genes in PRC2-inactivated MPNST cell lines treated with I-BET151 were identified using DESeq2 (RRID: SCR_015687; ref. 35) with the Wald test and apeglm (RRID: SCR_015687; ref. 36). Genes with an adjusted P value <0.05 were considered differentially expressed. Heatmaps were created using the pheatmap package. The code used for generating the different bioinformatic analyses performed can be found at: https://github.com/miriammagallon/RNA-seq_Sara_MPNSTcl_treatments.

Cell-cycle analysis

Cells were seeded and treated as for RNA extraction. After 20 hours, cells were fixed in 70% ethanol and incubated at −20°C for 24 hours. Cells were suspended in citrate phosphate buffer, incubated for 30 minutes at room temperature, dyed with PBS-1%, FBS, propidium iodide, and RNase A for 30 minutes at 37°C, and analyzed by flow cytometry. Each cell line was analyzed in three independent replicates.

Immunohistochemistry

IHC was carried out using the BenchMark ULTRA staining module, with the ultraView Universal DAB kit (760-500, Ventana Medical Systems). Each step was carried out automatically. Antigen retrieval was done with Cell Conditioning Solution 1, pH = 8 (950-124, Ventana Medical Systems). The tissues were blocked with 3% hydrogen peroxide and incubated with primary antibodies (CD68 and CD163, prediluted mouse monoclonal, Supplementary Table S3A) for 36 and 28 minutes, respectively. The primary antibody was localized using an horseradish peroxidase–conjugated secondary antibody with an enzyme, and the resulting complex was visualized with hydrogen peroxide and 3,3′-tetrahydrochloride diaminobenzidine chromogen.

Ethics statement

This scientific project has been developed in accordance with the Declaration of Helsinki and approved by the institutional review board (IRB). For the previous development of the PDOX models, written informed consent from the patients was obtained, and the study was approved by the IDIBELL IRB. All animal experiments were approved by the IDIBELL Animal Ethical Experimentation Committee (#9111), and the study passed IDIBELL IRB approval (#PR213/13).

Data availability

The RNA-seq data generated in this study are publicly available in the NF Data Portal in Synapse (https://doi.org/10.7303/syn61846182) and at the European Nucleotide Archive (accession: PRJEB83680;

https://www.ebi.ac.uk/ena/browser/view/PRJEB83680). Any additional information required to analyze the data reported in this article is available from E. Serra (corresponding author) upon request.

Results

Benchmarking MEKi, CDKi, and BETi and their combinations in MPNST cell lines through HTS

To explore the possibilities of precision medicine for MPNSTs based on TSG status, we first screened all MEKi, CDKi, and BETi present in the NIH MIPE 4.0 library (14 MEKi, 11 CDKi, and 3 BETi) on three different NF1-related MPNST cell lines: S462, NF1-08, and NF1-09. S462 and NF1-08 bore the inactivation of all three TSGs and were classified by methylome profile as MPNSTs (37), whereas NF1-09 is wild type (WT) for PRC2 function and was methylome-classified as an MPNST-like tumor (**Fig. 1A**; Supplementary Fig. S3). In addition, NF1-09 bore a *PIK3CA* activating mutation.

We assessed drug effects on cell viability using the CTG assay after 48 hours of treatment. Dose–response curves were obtained for all 28 single agents tested, and potency (AC_{50}) and % viability at the maximum concentration tested [maximum response (MAXR)] were used to classify compound activity on cell viability based on CRC (30, 38). **Figure 1A** presents a heatmap with MAXR values for each compound and cell line. The MAXR data show a high degree of redundancy among inhibitors of the same target class. Most inhibitors were active, although some compounds were not active in any cell line (e.g., MEKis: SL-327, U-0126, refametinib, and PD-098059; CDKis: purvalanol B and indirubin). S462 and NF1-08 cell lines responded more similarly to all compounds than the NF1-09 model (Supplementary Fig. S2). The NF1-09 cell line responded to CDKi single agents but slightly less sensitive to BETi, presumably because of the WT status of PRC2, and did not respond to MEKis. Based on the published work, we speculate that the *PIK3CA* activating mutation could be interfering with MEKi activity (39, 40). Control HFFs were used to assess generic toxicity, discarding two CDKis (fascaplysin and UCN-01).

Based on CRC scores (−1.1, −1.2, −2.1, and −2.2) and lack of toxicity, we selected 22 of the 28 agents for further testing in an all-versus-all pairwise combination screen. As a result, 147 discrete 10×10 dose–response matrices were tested in the three MPNST cell lines, using the CTG assay after 48 hours of treatment. We scored synergistic combinations using Delta Bliss Sum Negative and Excess HSA values (Supplementary Table S1). The more negative these two values, the more synergistic a combination is. As was seen for the single agent screening, high redundancy in the effect of drug combinations of compounds inhibiting the same target classes was observed (Supplementary Fig. S4). Based on combination synergy scores, degree of redundancy, and stage of clinical development, we selected 8 compounds in 21 combinations for further validation: three MEKis (ARRY-162, selumetinib, and trametinib), three CDKis (palbociclib, R-547, and flavopiridol), and two BETis (JQ1 and I-BET151). **Figure 1B** shows the Delta Bliss Sum Negative values of the 21 resulting combinations, all of them being synergistic combinations. An additional CDKi (ribociclib) not present in the MIPE 4.0 library was also selected for further validation based on their current use in the clinical practice and the good results obtained in a co-clinical pilot study (data not shown).

Identification of the three most synergistic combinations of selected MEKi, CDKi, and BETi in a panel of nine MPNST cell lines

We next performed an *in vitro* validation of the results obtained in the HTS. Instead of using CTG, 3-[4,5-dimethylthiazol-2-yl]-2,5 diphenyl tetrazolium bromide assay was performed as a cell viability readout in treatments combining the nine selected drugs (eight selected from the HTS plus ribociclib), in all possible combinations of drugs with different target classes (MEKi vs. CDKi, CDKi vs. BETi, and MEKi vs. BETi), generating a total number of 26 combinations. First, all combinations were tested in a panel of three NF1-related MPNST cell lines bearing the three inactivated TSGs (S462, NF1-08, and sNF96.2), and combination indexes (CI) were calculated for all of them according to dose–response curves (Supplementary Table S4). Although most combinations were synergistic in the three MPNST cell lines tested, the degree of synergism was different for each cell line. In the case of S462, 23 of the 26 combinations had CIs lower than 0.9 in fractions affected greater than 0.9 (Supplementary Table S4; Supplementary Material S1), demonstrated to be the most sensitive cell line. NF1-08 and sNF96.2 cell lines exhibited similar and lower sensitivities than S462, with only 13 and 14 of the 26 combinations, respectively, showing CIs lower than 0.9 at fractions affected greater than 0.9 (Supplementary Table S4; Supplementary Material S1). All combinations of MEKi–BETi were synergistic in the three MPNST cell lines used, whereas many MEKi–CDKi co-treatments were not synergistic in the NF1-08 and sNF96.2 cell lines. These results are consistent with responses obtained using single agent treatments.

The 12 most synergistic combinations were also tested in the HFF cell line to assess toxicity (Supplementary Material S1). Only the combination of palbociclib with I-BET151 exhibited significant toxicity and was discarded for further investigation. From the remaining 11 combinations, we selected two combinations of each pair of inhibitor classes (MEKi–CDKi; MEKi–BETi; CDKi–BETi), making a total of six combinations that were further validated in six additional MPNST cell lines (NF1-09, NF1-18B, ST88-14, NMS-2, NF90-8, and SP-10; **Fig. 1A**; Supplementary Fig. S3). The six cell lines have mutations in the three TSGs (*NF1*, *CDKN2A*, and PRC2), except for NF1-09, which is WT for PRC2, and they are classified as MPNST by methylome profile (**Fig. 1A**; refs. 12, 15, 37). The data from the six drug combinations tested in nine independent MPNST cell lines are shown in Supplementary Material S1. The six combinations exhibited synergism across the cell lines. Finally, a member of each class of inhibitors was selected to be used *in vivo*, based on the general synergism exhibited and their clinical development status: ARRY-162 (MEKi also known as binimetinib), ribociclib (CDKi), and I-BET151 (BETi; **Fig. 2**; Supplementary Fig. S5). **Figure 2A** presents the synergy of the three selected combinations across the nine MPNST cell lines tested, whereas **Fig. 2B** shows the CI values for each of the five doses tested in the MPNST lines. In most cell lines, almost all doses tested were synergistic, many of them affecting cell viability by greater than 50%, with the combination of ARRY-162 + I-BET151 being the most synergistic one.

The MEKi–BETi combination ARRY-162 + I-BET151 elicits *in vivo* tumor shrinkage in sporadic and NF1-associated MPNST PDOX

We next tested the three selected combinations (ARRY-162/I-BET151, ARRY-162/ribociclib and I-BET151/ribociclib) *in vivo* using two MPNST PDOX models: one NF1-associated (NF1-18B) and one sporadic (SP-10) generated using tumors from our MPNST preclinical platform (11, 12). Treatment groups consisted of 9 to 10 mice receiving either vehicle, single treatments or their combinations (for the NF1 MPNST PDOX model, single treatments consisted of groups of five mice).

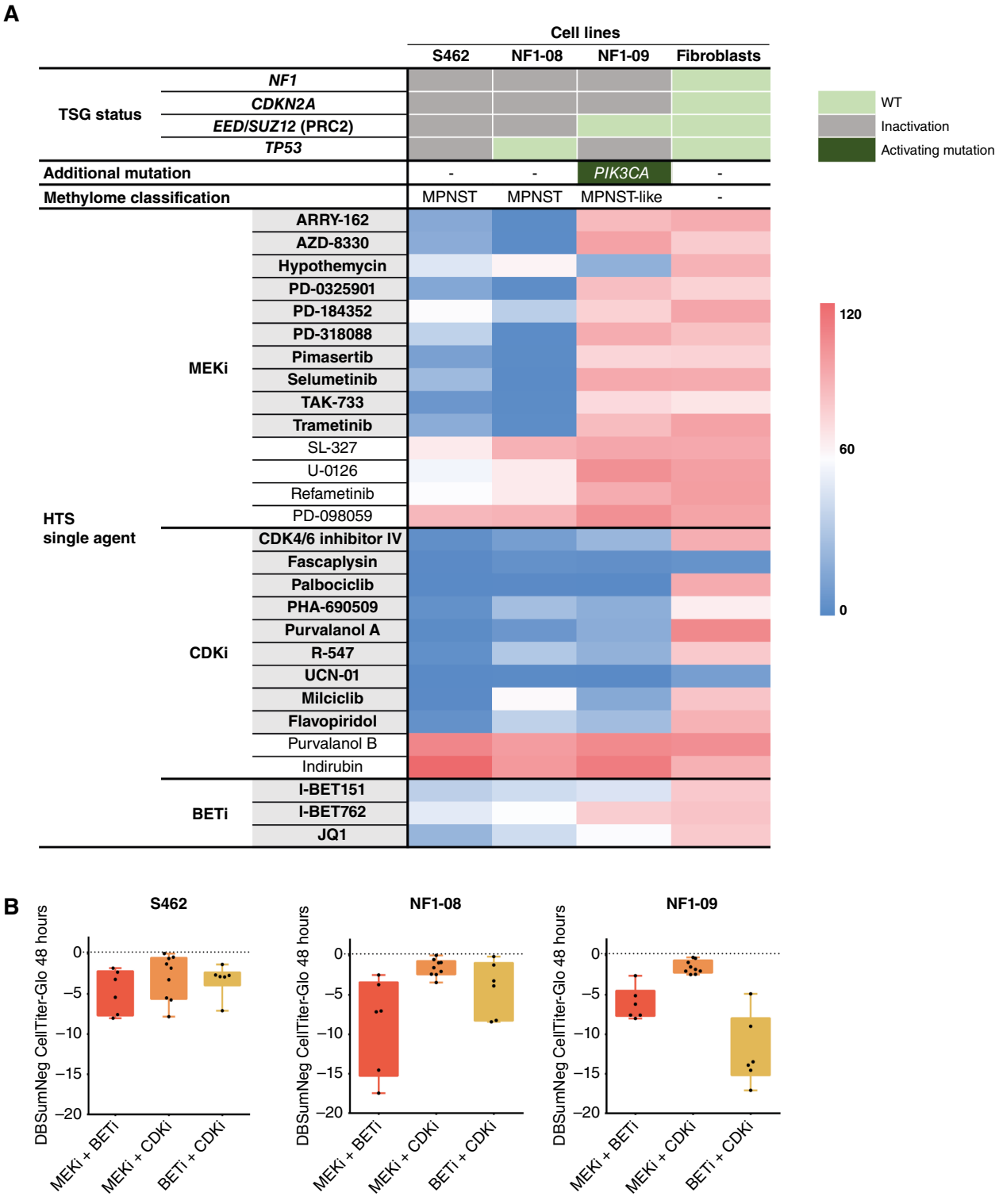

Figure 1.

HTS of MEKi, CDKi, and BETi from the MIPE 4.0 library as single agents and as pairwise combinations. **A,** Heatmap plot representing the cellular mutational status information and the result of the HTS as single agents in the three MPNST cell lines used (S462, NF1-08, and NF1-09) and in a fibroblast (HFF) cell line as the toxicity control. The heatmap using MAXR values as % cell viability. The 22 compounds selected for validation in combination are highlighted in gray. **B,** Delta Bliss Sum Negative (DBSumNeg) values for cell viability at 48 hours of the 21 selected synergistic combinations separated in groups of treatments in the three MPNST cell lines used. Each black dot indicates one single value.

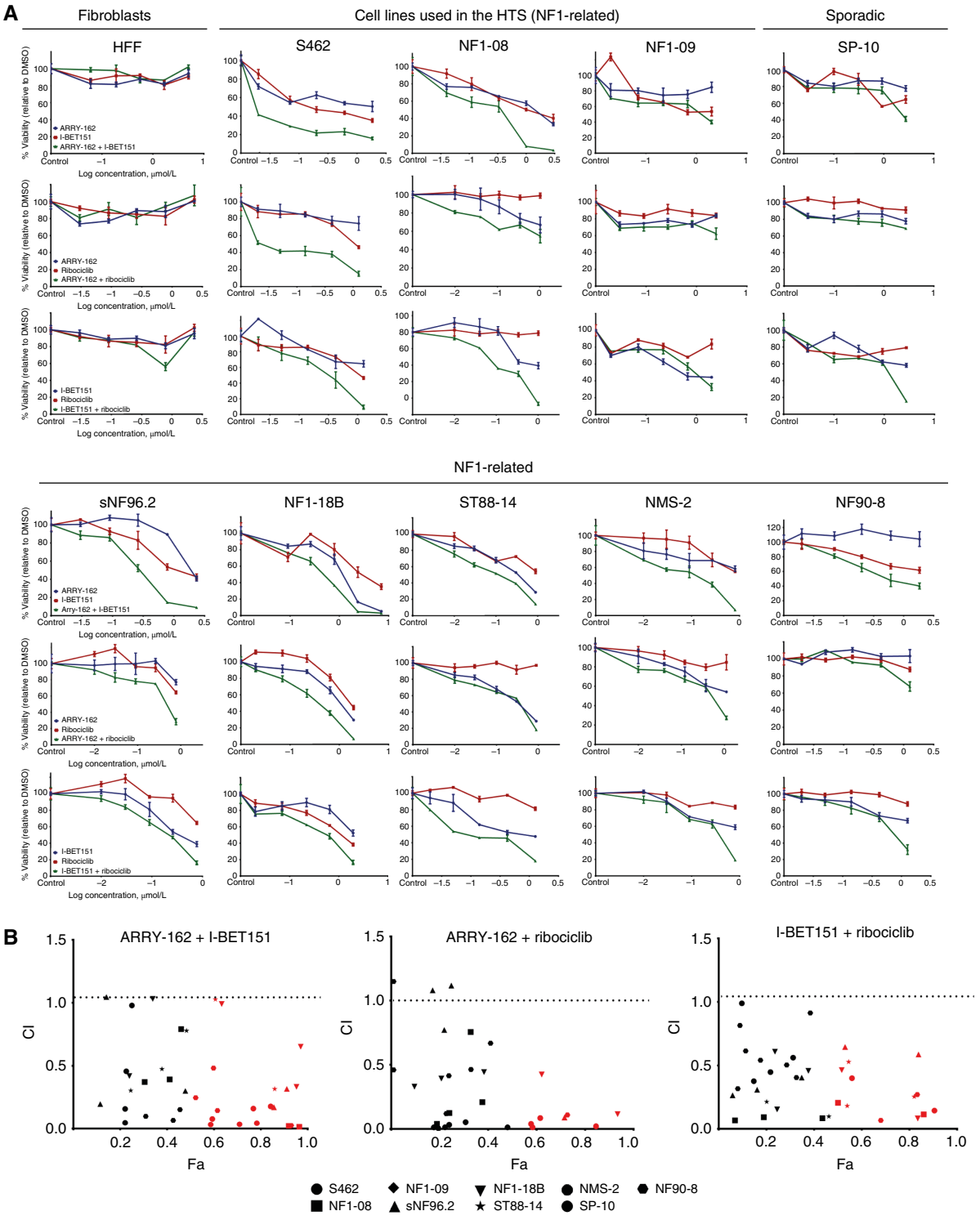

Figure 2.

In vitro testing of the three most synergistic combinations in a large panel of MPNST cell lines. **A,** Single agent and combined responses for the three selected combinations reported by the 3-[4,5-dimethylthiazol-2-yl]-2,5 diphenyl tetrazolium bromide (MTT) viability assay in nine MPNST cell lines and a fibroblast (HFF). **B,** CI plots of the three selected combinations at several doses showing the fraction affected (Fa) vs. the CI of the nine MPNST cell lines used. Fa values represent the fraction of cell death by drug treatment, ranging from 0 (no cell death) to 1 (100% cell killing). CI values lower than 0.9 indicate a synergistic combination, CI values between 0.9 and 1.1 indicate an additive effect, and values higher than 1.1 indicate antagonistic effect. In black are the points with Fa lower than 0.5, and in red are the values with Fa greater than 0.5.

In the NF1-associated PDOX model, for the I-BET treatment, we started with a dose of 25 mg/kg, three times per week, a bit lower than the defined MTD of 30 mg/kg, daily, based in our previous experience comparing nude mice with or without tumors (23). The combination of ARRY-162/I-BET151 elicited the best treatment response, decreasing tumor growth rate and even reducing tumor volume in half of the mice after 2 weeks of treatment (**Fig. 3A** and **B**). A reduction in tumor weight by 75% with this combination treatment compared with controls was observed at the end of the treatment, confirming volume measurements (**Fig. 3C** and **D**; Supplementary Fig. S6A). The other two combinations tested (ARRY-162 + ribociclib and I-BET151 + ribociclib) also decreased tumor growth rate but did not arrest tumor growth. No toxicity was observed for any of the combinations during the 2 weeks of treatment (**Fig. 3E**).

To assess the effect of drug combination *in vivo*, we used Western blot analysis to analyze the status of relevant signaling pathways or known biomarkers of treatment responses (**Fig. 3F**). For MEKi, we interrogated the reduction of p-ERK (17). For CDK4/6 inhibitors, we analyzed p-RB (19) and WEE1 (41). Treatment response to BETi was assessed analyzing MYC levels (42). Both combinations containing MEKi ARRY-162 showed a significant reduction of p-ERK compared with vehicle-treated controls, confirming the inhibition of the MAPK pathway. Both combinations containing ribociclib decreased p-RB/RB ratio and WEE1 levels, indicating an effect on cell-cycle regulation. Finally, we observed a statistically significant reduction of MYC expression in ARRY-162 + I-BET151 combination and a clear reduction in the I-BET151 + ribociclib combination, although it was not statistically significant (**Fig. 3F**).

In the sporadic PDOX model, the combination of ARRY-162 + I-BET151 also produced the most efficacious response, reducing the tumor volume by 65% after 2 weeks of treatment (**Fig. 4A** and **B**). Tumor weight after excision was reduced by 90% compared with the vehicle control group (**Fig. 4C** and **D**; Supplementary Fig. S6B). The other two combinations also decreased the tumor growth rate, even more than in the NF1-related model, but did not produce tumor size reduction. As we did not observe I-BET151–related toxicity in the NF1 model, we increased the dose of I-BET151 to 30 mg/kg, daily, as concluded in the MTD test. However, during the first week of treatment both co-treatments including I-BET151 showed some toxicity, indicated by mice weight loss (**Fig. 4E**). Thus, we followed the same dosage regimen as the NF1 model during the second week of treatment, observing weight recovery (**Fig. 4E**). Moreover, we performed another experiment to observe tumor regrowth after 3-week treatment with ARRY-162 + I-BET151. Tumors had a mean volume of 500 mm^3 when treatment stopped, and 2 weeks later, the volume increased to 1,200 mm^3 (**Fig. 4F**). We then restarted treatment for three more weeks using the same dosage regimen and achieved a reduction in tumor volume by 50% (**Fig. 4F**).

We also assessed drug activity molecularly, as described above. For all combination treatments of ARRY-162, there was a statistically significant difference in p-ERK levels between vehicle-treated control group and co-treated groups (**Fig. 4G**). Both combinations containing ribociclib decreased p-RB/RB ratio and WEE1, although only the reduction in WEE1 levels was statistically significant in both combinations. Finally, we observed a statistically significant reduction of MYC expression in the ARRY-162 + I-BET151 co-treatment and a clear reduction in the I-BET151 + ribociclib combination (**Fig. 4G**).

Evaluating the impact of the MEKi–BETi co-treatment on tumor response

We further investigated the mechanism by which MEKi–BETi treatment induces PDOX tumor reduction by exploring their impact on gene expression, cell proliferation, and apoptosis. We first aimed to evaluate its effects on the reversion of gene expression signatures caused by the loss of PRC2 function. For that, we treated three cell lines WT for PRC2 (NF1-09, HS-Sch-2, and STS-26T) and three MPNST cell lines deficient for PRC2 (S462, SP-10, NF1-18B) with I-BET151 as a single agent in both groups and in combination with ARRY-162 in the PRC2-deficient cells. After 20 hours of treatment, we extracted RNA and performed bulk RNA-seq (**Fig. 5A**). We performed a PCA on all treated and untreated cell lines (**Fig. 5B**) and observed that global expression variation among samples was dominated by the functional status of PRC2, clearly separating PRC2-active from PRC2-inactive cell lines. PCA also revealed that the perturbation of transcriptional profiles in PRC2-mutated cell lines by either I-BET151 treatment alone or by the ARRY-162 + I-BET151 combination was quite small and similar to the effect of these inhibitors in PRC2 WT cells (**Fig. 5B**). We then performed a differential gene expression analysis comparing I-BET151-treated versus untreated PRC2-deficient cell lines and plotted differentially expressed genes for all experimental conditions in a heatmap (**Fig. 5C**). We obtained a transcriptional signature of upregulated and downregulated genes, very few specific to PRC2-inactivated cell lines. The small number of genes precluded performing an enrichment analysis. We further analyzed several selected genes as potential biomarkers of BETi treatment response, including *TPPP* and *NGFR* as upregulated genes and *PRDM1* as a downregulated gene, by RT-qPCR (Supplementary Fig. S7) and by performing Western blotting on treated cell lines and tumors (**Fig. 5D** and **E**). Altogether, the differences observed comparing mRNA and protein levels *in vitro* and *in vivo* impeded to reach any conclusion. The way MEKi–BETi co-treatment was eliciting tumor reduction *in vivo* seemed not to be related to the transcriptional reversion of genes altered by the loss of PRC2 function.

Then we analyzed the cell cycle of MPNST cell lines untreated and treated with MEKi–BETi by flow cytometry. We observed a decrease in the proportion of cells at the S-phase and an increase in the G_1-phase, denoting cell-cycle arrest for both BETi treatment and MEKi–BETi co-treatment (**Fig. 5F**). We then evaluated the number of mitotic cells present in treated versus untreated PDOX *in vivo* with the three selected combinations (**Fig. 5G**). In both the sporadic and NF1-related PDOXs, there was a statistically significant reduction in the number of mitoses in the three treatments, particularly in the MEKi–BETi–treated tumors. These results were consistent with the reduced tumor growth rate elicited by the different co-treatments but did not fully explain tumor shrinkage in all sporadic cases and half of the NF1-related PDOX. Thus, we next analyzed BIM-associated apoptosis (21, 43) and activation of downstream caspases in three MPNST cell lines. BETi treatment and MEKi–BETi co-treatment caused a consistent increase in BIM expression in three independent MPNST cell lines (**Fig. 5H**). We also analyzed BIM expression in treated and control MPNST PDOXs. Although the NF1-associated co-treated PDOX showed a clear increase in BIM expression, this increase was modest in the sporadic PDOX (**Fig. 5I**). Neither in the cell lines nor in the PDOX models treated with ARRY-162 + I-BET151, we were able to detect cleaved caspases 3, 7, and 9 (data not shown).

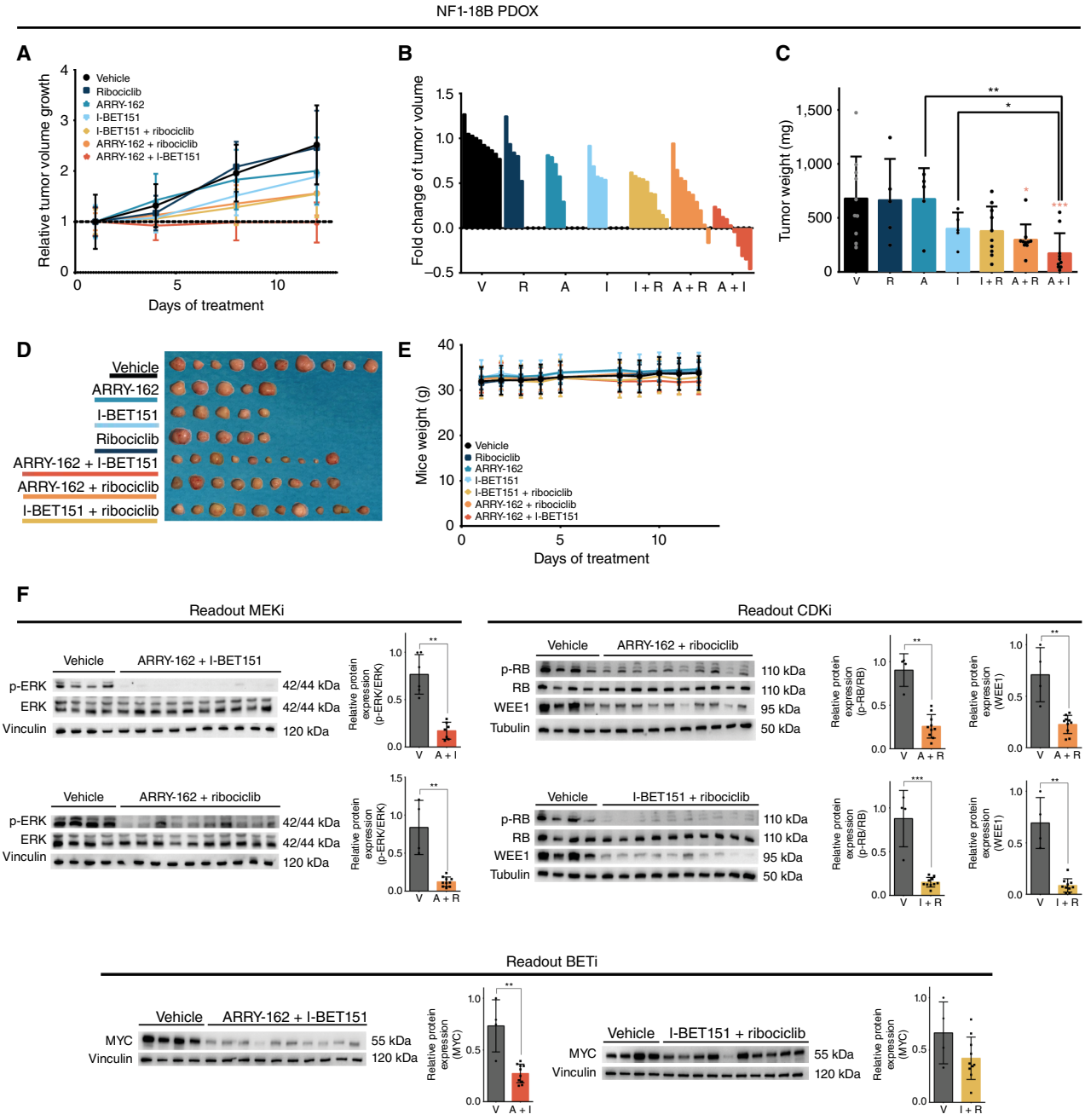

Figure 3.

In vivo testing of the three selected combinations in the NF1-associated MPNST PDOX mouse model. **A,** Relative tumor volume growth of the NF1-18B PDOX mouse model during the 2 weeks of treatment in each group. **B,** Waterfall plot of the fold change of each individual tumor at the end of the experiment. **C,** Tumor weight at the end of the experiment (Mann–Whitney test). Each black dot indicates one single value. **D,** Photographs of the collected tumors at the end of the experiment. **E,** Plot of the mice weight during the 2 weeks of treatment. **F,** Analyses of the molecular targets of ARRY-162 (p-ERK/ERK), ribociclib (p-RB/RB and WEE1), and I-BET151 (MYC) using Western blotting. Mann–Whitney test: ***, *P* value ≤ 0.001; **, *P* value ≤ 0.01; *, *P* value ≤ 0.05. A, ARRY-162; A + I, ARRY-162 + I-BET151; A + R, ARRY-162 + ribociclib; I, I-BET151; I + R, I-BET151 + ribociclib; R, ribociclib; V, vehicle.

Finally, we analyzed physiologic changes in the tumor microenvironment caused by the co-treatments. Considering the compromised immune system of the athymic nude mice used, with no mature T cells, but presenting viable macrophages, and based also on previous results (44), we performed a histologic analysis using CD68 and CD163 to detect macrophage infiltration in two independent MPNST PDOXs, from the control group and each of the *in vivo* co-treatments performed (Supplementary Fig. S8). The three co-treatments induced the loss of M2 macrophages (stained using CD163) in both MPNST PDOX models, as previously observed in genetically engineered

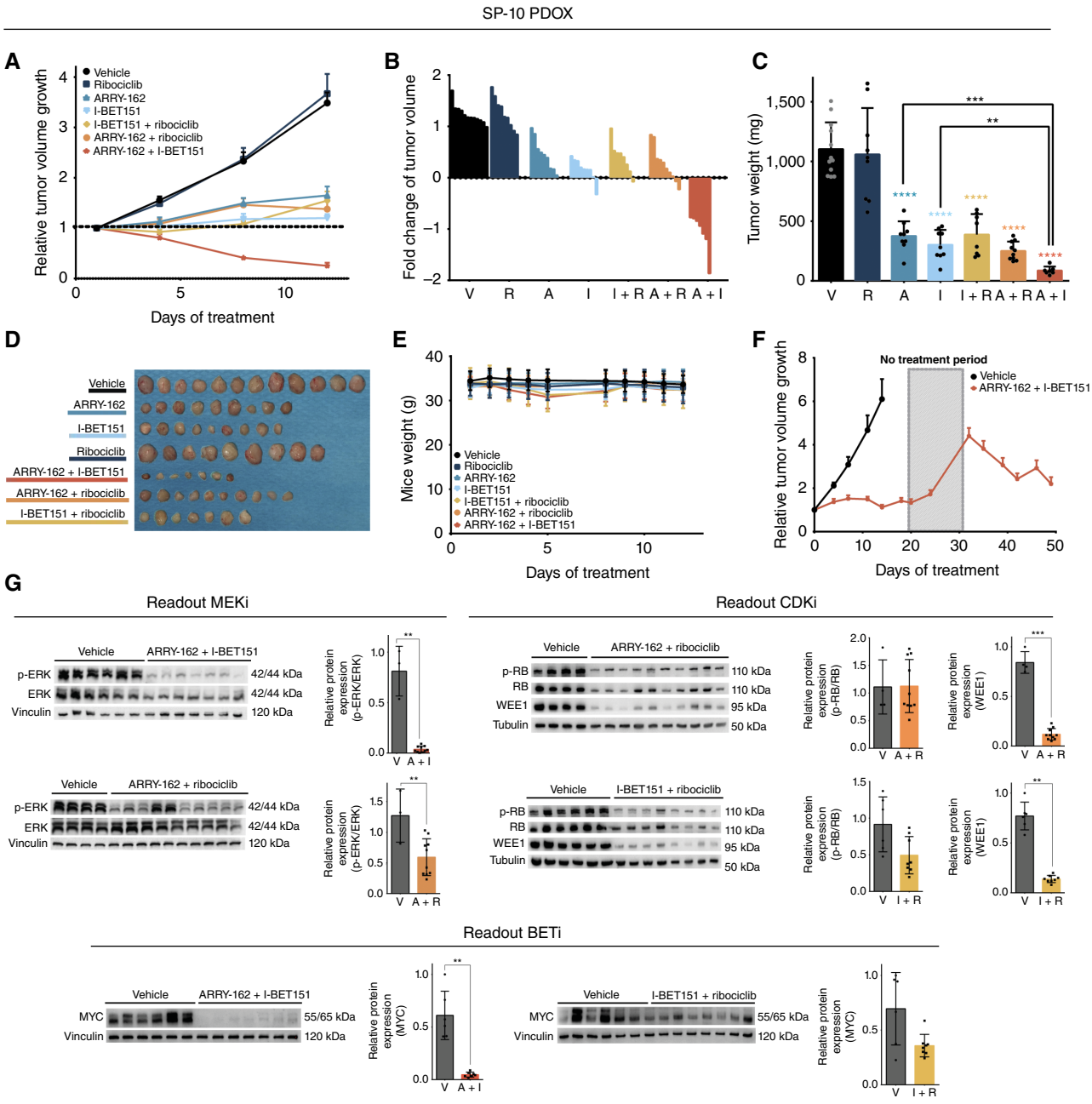

Figure 4.

In vivo testing of the three selected combinations in the sporadic MPNST PDOX mouse model. **A,** Relative tumor volume growth of the SP-10 PDOX mouse model during the 2 weeks of treatment in each group. **B,** Waterfall plot of the fold change of each individual tumor at the end of the experiment. **C,** Tumor weight at the end of the experiment (Mann–Whitney test). Each black dot indicates one single value. **D,** Photographs of the collected tumors at the end of the experiment. **E,** Plot of the mice weight during the 2 weeks of treatment. **F,** Relative tumor volume growth of the SP-10 PDOX mouse model during the regrowth experiment treated with ARRY-162 + I-BET151. **G,** Analyses of the molecular target of ARRY-162 (p-ERK/ERK), ribociclib (p-RB/RB and WEE1), and I-BET151 (MYC) using Western blot analysis. Mann–Whitney test: ****, *P* value ≤ 0.0001; ***, *P* value ≤ 0.001; **, *P* value ≤ 0.01; *, *P* value ≤ 0.05. A, ARRY-162; A + I, ARRY-162 + I-BET151; A + R, ARRY-162 + ribociclib; I, I-BET151; I + R, I-BET151 + ribociclib; R, ribociclib; V, vehicle.

mouse models (44). We detected differences in the number of macrophages present in both control nontreated groups, suggesting a probable change in the tumor microenvironment upon MEKi–BETi co-treatment and specific microenvironment cell compositions in each PDOX.

The triple combination of MEKi–BETi–CDKi further increases the reduction of tumor volume, reaching tumor disappearance in some cases

Results obtained with the MEKi–BETi combination, and the fact that most MPNSTs exhibit the inactivation of the three targeted

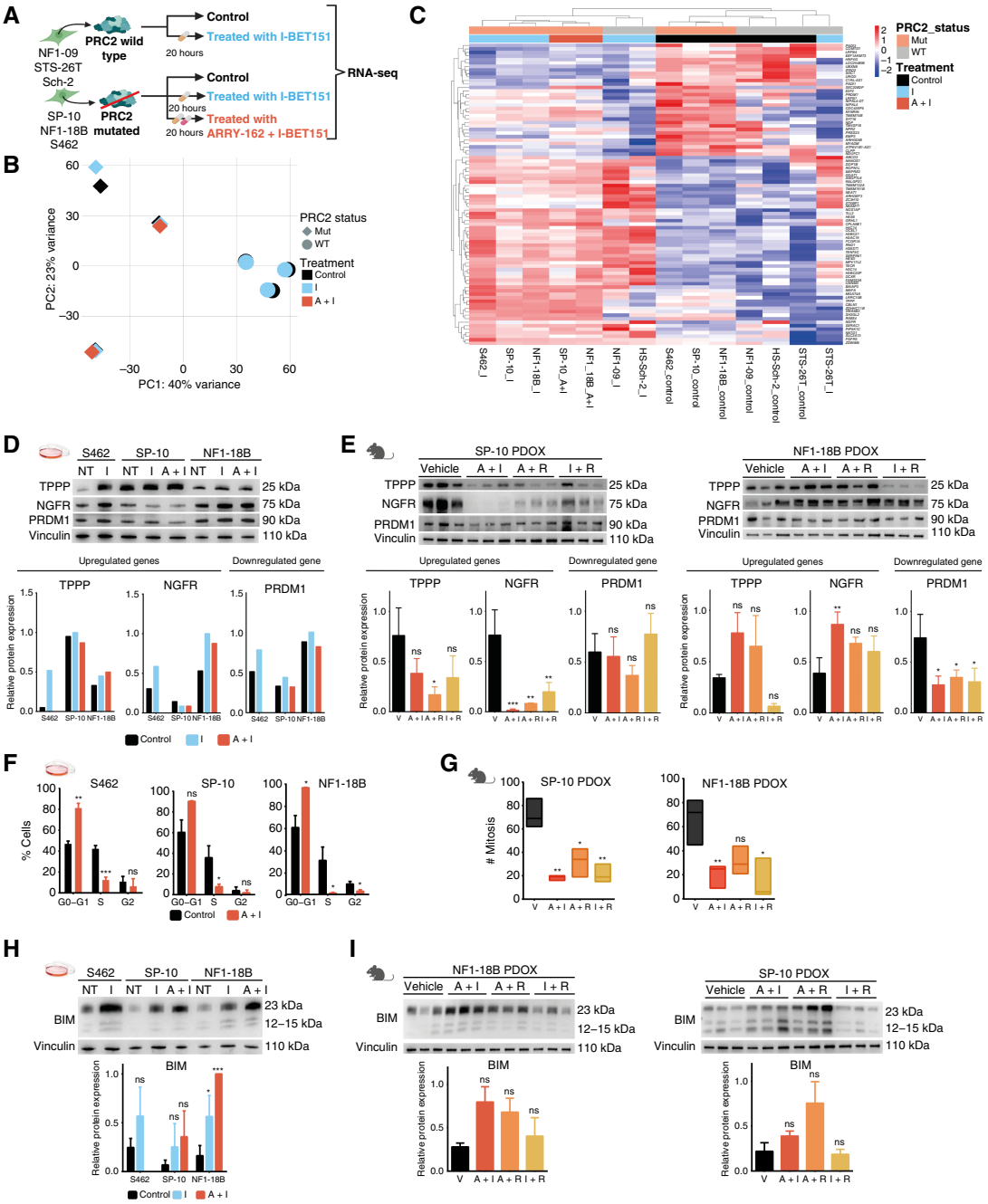

Figure 5.

Evaluating the impact of the MEKi–BETi co-treatment on tumor response. **A,** Schematic representation of the experimental design to analyze changes in gene expression upon I-BET151 and ARRY-162 + I-BET151 treatment. **B,** PCA plot showing the distribution of treated and untreated cell lines. The status of PRC2 is represented using different forms. Different treatments are represented in different colors. **C,** Heatmap representing differentially expressed genes of I-BET151 (I) treated vs. untreated cell lines for all cell lines and conditions analyzed. **D,** Protein expression analysis by Western blots and graphs of TPPP, PRDM1, and NGFR in three MPNST cell lines: untreated (control, NT) and treated with I-BET151 (I) or ARRY-162 + I-BET151 (A + I). **E,** Protein expression analysis by Western blots and graphs of TPPP, PRDM1, and NGFR in the NF1-18B and SP-10 PDOX models after co-treatments. **F,** Percentage of cells in each phase of the cell cycle in three MPNST cell lines (S462, SP-10, and NF1-18B) treated with DMSO (control) or with ARRY-162 + I-BET151 (A + I; $n = 1$). **G,** Number of mitoses in a 1.7 mm^2 area of a hematoxylin and eosin staining. **H,** Western blot analyses and plot of BIM protein expression in three MPNST cell lines: control and treated with I-BET151 or ARRY-162 + I-BET151. **I,** Western blot analyses and graph of BIM protein expression in the tumors of NF1-18B and SP-10 PDOX models after treatments. The Tukey test was used for the statistics, in which each treatment group was analyzed against its control: ***, P value ≤ 0.001; **, P value ≤ 0.01; *, P value ≤ 0.05. A + I, ARRY-162 + I-BET151; A + R, ARRY-162 + ribociclib; I, I-BET151; I + R, I-BET151 + ribociclib; Mut, PRC2-inactivated; NRE, normalized relative expression; NT, no treatment; V, vehicle. Note that NGFR/PRDM1 data from **Fig. 5E** and BIM data from **Fig. 5I** were run on the same immunoblot, sharing the same vinculin blot. (**A,** Created in BioRender. Creus, E. [2024] https://BioRender.com/p71e952.)

TSGs, prompted us to perform a final *in vivo* assay, comparing the MEKi–BETi combination with the triple combination of inhibitor classes. We used the same two PDOX models but started treatments when tumors were a bit smaller than those used in the previous MEKi–BETi assays, to allow a longer period of treatment before MPNSTs treated with vehicle reached a maximum tolerated size and mouse had to be sacrificed. In the NF1-associated MPNST model (NF1-18B), the triple combination led to a 50% reduction in tumor volume compared with the MEKi–BETi combination after 3 weeks of treatment (**Fig. 6A** and **B**). The analysis of tumor weight showed that although vehicle-treated tumors weighed 1,942 mg on average, those treated with MEKi–BETi combination weighed 310 mg on average and with the triple treatment weighed 218 mg on average, confirming volume measurements (**Fig. 6C** and **D**; Supplementary Fig. S9A). Importantly, no toxicity was observed throughout the 3-week treatment period (**Fig. 6E**). Tumors from four of eight mice were analyzed, whereas the remaining four mice were monitored for tumor regrowth after drug withdrawal. Tumor size was measured weekly during a month, and regrowth was observed in all four mice already after 2 weeks of treatment cessation (**Fig. 6F**).

We then replicated this *in vivo* study in the sporadic MPNST PDOX model (SP-10). In this model, we observed an almost 85% overall average reduction in tumor volume compared with baseline (**Fig. 6G** and **H**). Furthermore, significant differences were also observed when comparing the final tumor weights (**Fig. 6I** and **J**; Supplementary Fig. S9B). The vehicle-treated group weighed 2,041 mg on average, MEKi–BETi combination weighed 122 mg on average, and MEKi–BETi–CDKi–treated tumors weighed 29 mg on average. Notably, in two of the eight mice treated with the triple combination for 3 weeks, tumors were undetectable by palpation. To investigate whether there was a complete tumor clearance, we performed a hematoxylin and eosin staining of the femoral biceps of one of these mice after sacrifice, detecting small residual tumor tissue (**Fig. 6J**). As with the NF1-18B model, no toxicity of the MEKi–BETi–CDKi co-treatment was observed in the mice (**Fig. 6K**). The other mouse with no palpable tumor, together with the three remaining mice, was used for a tumor regrowth assay (**Fig. 6L**). One of the mice exhibited tumor regrowth at 20 days after treatment cessation, whereas two others exhibited a much slower tumor regrowth (**Fig. 6L**). Remarkably, in the mouse with no palpable tumor, no tumor recurrence was observed even 1 month after treatment discontinuation (**Fig. 6L**).

To assess the activity of drugs in the reduction of tumors, we performed Western blot analyses on ~4 tumors per condition and PDOX model to monitor the status of targeted signaling pathways (Supplementary Figs. S10 and S11). In all cases, we detected the effect of drugs on pathway inhibition, with the sporadic MPNST model (SP-10) exhibiting a greater generalized pathway inhibition compared with the NF1-associated model (NF1-18B).

Discussion

With the aim of identifying new therapeutic opportunities for patients with MPNSTs, we developed a preclinical platform consisting in different MPNST cell lines and PDOX mouse models, histologically and genomically characterized and validated by comparison with the original tumors (11, 12). This preclinical platform can be used for assaying compounds selected from library screenings, testing precision medicine strategies, or developing personalized co-clinical treatments (23, 45).

The analysis of the HTS data performed in this work allowed us to benchmark a large number of different inhibitors of the same targets (MEKi, CDKi, and BETi) present in the NCATS MIPE 4.0 library, facilitating a comprehensive assessment of their effect on biologically diverse MPNST cell lines. We found a high degree of redundancy among inhibitors of the same class, despite specific sensibilities in certain MPNST cell lines. This redundancy was consistent also when screening combinations of agents from the same classes. Identified synergies of pairwise drug combinations in HTS assays were validated in a broad panel of nine MPNST cell lines. The use of a high variety of biological replicates robustly supported the *in vitro* synergistic effects observed and allowed identifying some differences between cell lines despite bearing the three TSGs inactivated (**Fig. 2A**; ref. 17). Thus, there is a main role played by the mutational status of *NF1*, *CDKN2A*, and PRC2 in the responses to MEKi, CDKi, and BETi combinations, although there are other genetic, epigenetic, or physiologic differences that may modify treatment responses (46). Few compounds and combinations tested failed to confer any adverse effect on MPNST cell lines. We did not further investigate the underlying causes of this innocuous effect, with possible reasons being both a limited activity of the compounds and a technical issue in the assays performed.

Several combinations were also tested in a human nontumoral fibroblast cell line as control noncancer cells, to avoid potential secondary effects when testing the drugs preclinically *in vivo* or when they may arrive to patients. The combination of palbociclib (CDKi) and I-BET151 (BETi) elicited significant toxicity in the HFF cell line. Thus, we discarded it for the *in vivo* analysis. These results are important, as in our experience, *in vitro* toxicities in HFFs inform that the window between toxicity and effectivity could be narrow when translating *in vitro* to *in vivo* treatments, like when combining panobinostat (histone deacetylase inhibitor) with proteosome inhibitors or mTORC1 inhibitors (23). Furthermore, even if no toxicity is detected *in vitro* in HFFs, the final dosing regimen is key for identifying an effective treatment window between toxicity and effectivity *in vivo*, as was the case of the MEKi–BETi combination.

As we tested cell lines and PDOX models both derived from the same primary tumors and sharing the same genomics, we were able to compare *in vitro* and *in vivo* responses of models sharing almost the same genetic content. Surprisingly, there was not a good agreement between *in vitro* and *in vivo* responses. Although the SP-10 model *in vitro* was generally not very sensitive to any of the treatments (**Fig. 2A**), it was the most responsive tumor *in vivo* (**Fig. 4**), which is different to what was observed for the NF1-18B model, being clearly sensitive *in vitro* and a bit less responsive *in vivo* compared with the sporadic model. Differences between *in vitro* and *in vivo* treatment efficacies have already been reported by others (47). In our case, we think that at least part of the differences observed in *in vitro–in vivo* pair models may be explained by not only the direct effect of treatments on tumor cells but also their effect on the tumor microenvironment (48). In fact, we identified drug effects on both tumoral cells and the microenvironment acting concurrently. Although reversion of transcription changes produced by PRC2 loss upon BETi treatment seems not to play a role in tumor cells, METi–BETi co-treatment elicits a cytostatic effect, highly reducing tumor cell proliferation and some BIM-dependent apoptosis (21). In addition, a change in the composition of the immune microenvironment, exemplified by a reduction of M2 macrophages, could be also key in the observed PDOX reduction, supporting the addition of immunotherapy for treating

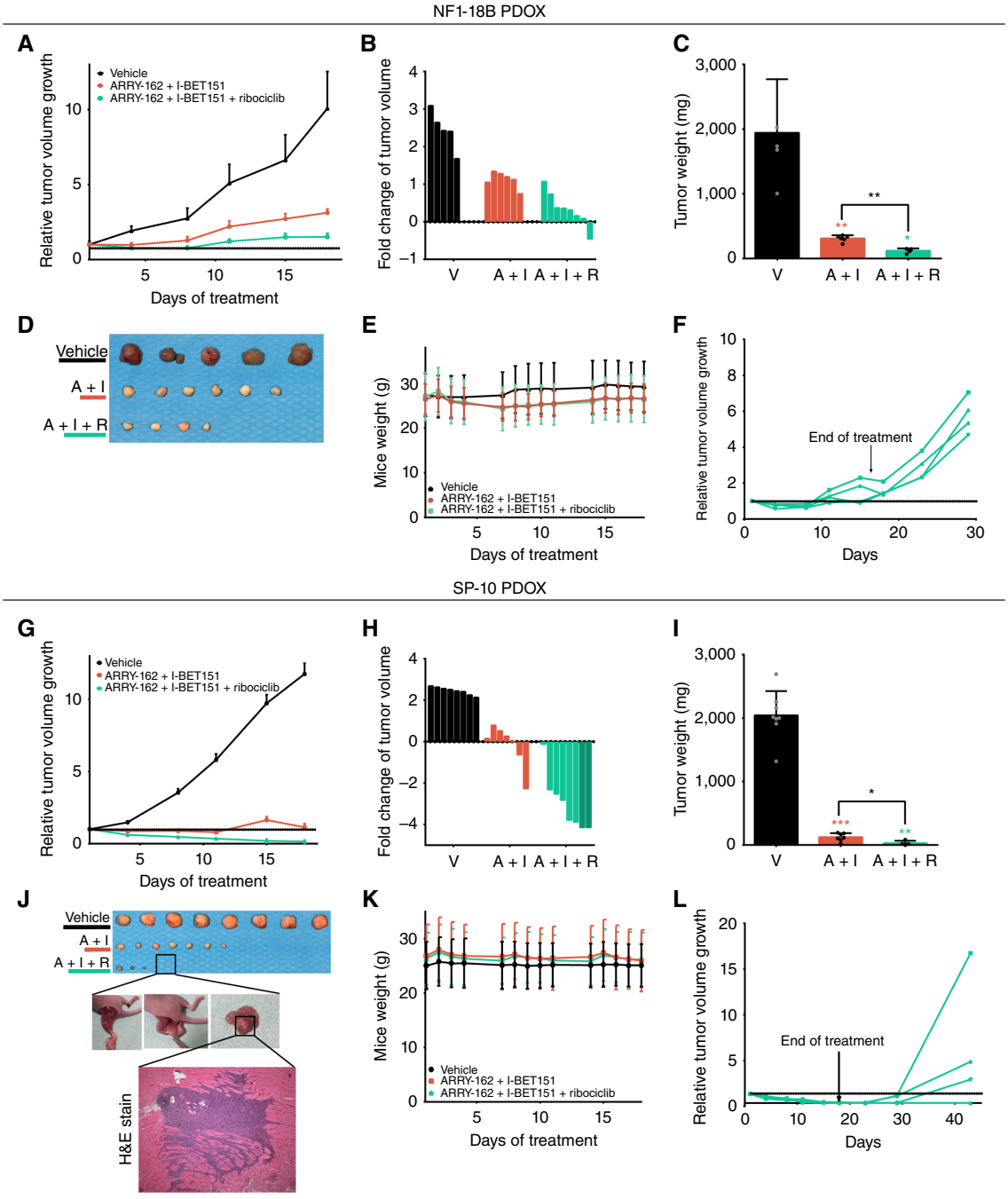

Figure 6.

In vivo testing of the triple combination of MEKi–BETi–CDKi in both MPNST PDOX mouse models: NF1-related (**A–F**) and sporadic (**G–L**). **A,** Relative tumor volume growth of the NF1-18B PDOX model during 3 weeks of treatment. **B,** Waterfall plot of the fold change of each individual tumor at the end of the experiment. **C,** Tumor weight at the end of the experiment (Mann–Whitney test). Each black dot indicates one single value. **D,** Photographs of the collected tumors at the end of the experiment. **E,** Plot showing mice weight during the 3 weeks of treatment. **F,** Analysis of tumor regrowth after the end of triple combination treatment. Relative tumor volume growth for four individual tumors is shown. **G,** Relative tumor volume growth of the SP-10 PDOX model during 3 weeks of treatment. **H,** Waterfall plot of the fold change of each individual tumor at the end of the experiment. The two darker green bars represent tumors that disappeared by palpation and were not measurable (final volume of 0). **I,** Tumor weight at the end of the experiment (Mann–Whitney test). Each black dot indicates one single value. **J,** Photographs of the collected tumors at the end of the experiment. Hematoxylin and eosin (H&E) staining of the femoral biceps of one of the mice without a palpable tumor, showing traces of tumor tissue. Image magnified 4×. **K,** Plot showing mice weight during the 3 weeks of treatment. **L,** Analysis of tumor regrowth after the end of triple combination treatment. Relative tumor volume growth for four individual tumors is shown. Note that no tumor recurrence was observed in one case. Mann–Whitney test: ***, *P* value ≤ 0.001; **, *P* value ≤ 0.01; *, *P* value ≤ 0.05. A + I, ARRY-162 + I-BET151; A + I + R, ARRY-162 + I-BET151 + ribociclib; V, vehicle.

MPNSTs under MEKi–BETi treatment (44). However, further analyses of changes in the tumor microenvironment upon METi–BETi co-treatment are required to properly understand how MPNST PDOXs are reduced.

In vivo combination treatments using two MPNST PDOX models, one sporadic and one NF1-associated, showed that the MEKi–BETi combination elicits a potent response in MPNST PDOX, stopping tumor growth and reducing tumor volume in half of the NF1 PDOX tumors (**Fig. 3**) and in all tumors of the sporadic PDOX model (**Fig. 4**). Previously published studies also showed a good response to MEKi–BETi co-treatments in MPNSTs arising in genetically engineered mouse models (20). However, the triple combination of inhibitor classes, MEK–BET–CDK, resulted in the best tumor PDOX response obtained so far, reaching disappearance in a few tumors during the assay period (**Fig. 6**) and not causing toxicity in treated mice. This important result will need to be extended to other MPNST PDOX models to assess the potential of this triple combination as a generalized therapy for MPNSTs, at least for those with the triple inactivation of TSGs. These results clearly support the use of precision medicine for MPNSTs. The observed differences in the MEKi–BETi co-treatment tumor responses to the first combination and the final triple treatment experiments could be explained by experimental differences, particularly by the initial bigger size of PDOX and the higher initial concentration of BETi in the first co-treatment experiment. In addition, there seems to be a better response of sporadic MPNSTs compared with NF1-derived MPNSTs when using these precision oncology–combined treatments, consistent with other works (9). New experiments using additional sporadic and NF1 PDOX models are needed to explore the extent of this observation.

In summary, our results strongly support precision therapies for MPNSTs guided by TSG inactivation status. MEKi–BETi–CDKi triple treatment elicits a significant reduction of human MPNST PDOXs, reaching PDOX MPNST disappearance in a few tumors after 3 weeks of treatment. This work provides valuable preclinical information for current and future clinical trials in humans.

Authors' Disclosures

I. Blanco reports other support from Alexion and SpringWorks outside the submitted work. C. Valverde reports personal fees and nonfinancial support from PharmaMar and Eli Lilly and Company; personal fees from Deciphera, Bayer, Philogen SpA, and Mundipharma; and grants and personal fees from Boehringer Ingelheim outside the submitted work. C. Romagosa reports personal fees from PharmaMar outside the submitted work. H. Salvador reports personal fees from Alexion during the conduct of the study. No disclosures were reported by the other authors.

Authors' Contributions

S. Ortega-Bertran: Conceptualization, data curation, formal analysis, investigation, visualization, methodology, writing–original draft, writing–review and editing. **J. Fernández-Rodríguez:** Conceptualization, investigation, writing–review and editing. **M. Magallón-Lorenz:** Data curation, software, formal analysis, visualization, writing–review and editing. **X. Zhang:** Investigation, writing–review and editing. **E. Creus-Bachiller:** Investigation, methodology, writing–review and editing. **A.P. Diazgranados:** Data curation, investigation, writing–review and editing. **I. Uriarte-Arrazola:** Investigation, methodology, writing–review and editing. **H. Mazuelas:** Investigation, methodology, writing–review and editing. **I. Blanco:** Resources, writing–review and editing. **C. Valverde:** Resources, writing–review and editing. **M. Carrió:** Investigation, methodology, writing–review and editing. **A. Villanueva:** Investigation, writing–review and editing. **T. De Raedt:** Investigation, writing–review and editing. **C. Romagosa:** Investigation, writing–review and editing. **B. Gel:** Data curation, software, formal analysis, writing–review and editing. **H. Salvador:** Resources, investigation, writing–review and editing. **M. Ferrer:** Resources, data curation, supervision, investigation, writing–review and editing. **C. Lázaro:** Conceptualization, resources, funding acquisition, investigation, project administration, writing–review and editing. **E. Serra:** Conceptualization, resources, supervision, funding acquisition, writing–original draft, project administration, writing–review and editing.

Acknowledgments

We thank all patients and families who donated MPNSTs to generate the preclinical therapeutic platform for MPNSTs. We would like to thank all Spanish patients with neurofibromatosis and neurofibromatosis associations for their continued support and effort, in particular the Spanish Asociación de Afectados de Neurofibromatosis and the Associacio Catalana de les Neurofibromatosis. We also wish to thank both pediatric and adult Spanish phakomatoses CSUR (Centros, Servicios y Unidades de Referencia) teams. This work has been supported mainly by Fundació la Marató de TV3 (51/C/2019). It has also been supported by the Carlos III National Institute of Health funded by FEDER funds—A Way to Build Europe (PI23/00017, PI23/00422, PI19/00553, and Centro de Investigación Biomédica en Red de Cáncer); the Department of Research and Universities of the Generalitat de Catalunya and AGAUR (Agència de Gestió d'Ajuts Universitaris i de Recerca; 2021SGR01112, 2021SGR00967); and Fundación Proyecto Neurofibromastosis. The publication/result/equipment/video/activity/contract/others is part of the project CPP2022-009550, funded by MCIU/AEI/10.13039/501100011033 and by the European Union "NextGenerationEU"/PRTR, with the institutional support provided by CERCA program/Generalitat de Catalunya.

Note

Supplementary data for this article are available at Clinical Cancer Research Online (http://clincancerres.aacrjournals.org/).

Received August 27, 2024; revised November 7, 2024; accepted December 23, 2024; published first December 30, 2024.

References

1. LaFemina J, Qin LX, Moraco NH, Antonescu CR, Fields RC, Crago AM, et al. Oncologic outcomes of sporadic, neurofibromatosis-associated, and radiation-induced malignant peripheral nerve sheath tumors. Ann Surg Oncol 2013;20:66–72.
2. Evans DG, Baser ME, McGaughran J, Sharif S, Howard E, Moran A. Malignant peripheral nerve sheath tumours in neurofibromatosis 1. J Med Genet 2002;39:311–4.
3. Ferner RE, Gutmann DH. International consensus statement on malignant peripheral nerve sheath tumors in neurofibromatosis. Cancer Res 2002;62:1573–7.
4. Uusitalo E, Rantanen M, Kallionpää RA, Pöyhönen M, Leppävirta J, Ylä-Outinen H, et al. Distinctive cancer associations in patients with neurofibromatosis type 1. J Clin Oncol 2016;34:1978–86.
5. Anghileri M, Miceli R, Fiore M, Mariani L, Ferrari A, Mussi C, et al. Malignant peripheral nerve sheath tumors: prognostic factors and survival in a series of patients treated at a single institution. Cancer 2006;107:1065–74.
6. Belakhoua SM, Rodriguez FJ. Diagnostic pathology of tumors of peripheral nerve. Neurosurgery 2021;88:443–56.
7. Le Guellec S, Decouvelaere AV, Filleron T, Valo I, Charon-Barra C, Robin YM, et al. Malignant peripheral nerve sheath tumor is a challenging diagnosis: a systematic pathology review, immunohistochemistry, and molecular analysis in 160 patients from the French Sarcoma Group Database. Am J Surg Pathol 2016;40:896–908.
8. Kim A, Lu Y, Okuno SH, Reinke D, Maertens O, Perentesis J, et al. Targeting refractory sarcomas and malignant peripheral nerve sheath tumors in a phase I/II study of sirolimus in combination with ganetespib (SARC023). Sarcoma 2020;2020:5784876.
9. Higham CS, Steinberg SM, Dombi E, Perry A, Helman LJ, Schuetze SM, et al. SARC006: phase II trial of chemotherapy in sporadic and neurofibromatosis type 1 associated chemotherapy-naive malignant peripheral nerve sheath tumors. Sarcoma 2017;2017:8685638.

10. Kim A, Stewart DR, Reilly KM, Viskochil D, Miettinen MM, Widemann BC. Malignant peripheral nerve sheath tumors state of the science: leveraging clinical and biological insights into effective therapies. Sarcoma 2017;2017:7429697.
11. Castellsagué J, Gel B, Fernández-Rodríguez J, Llatjós R, Blanco I, Benavente Y, et al. Comprehensive establishment and characterization of orthoxenograft mouse models of malignant peripheral nerve sheath tumors for personalized medicine. EMBO Mol Med 2015;7:608–27.
12. Creus-Bachiller E, Fernández-Rodríguez J, Magallón-Lorenz M, Ortega-Bertran S, Navas-Rutete S, Romagosa C, et al. Expanding a precision medicine platform for malignant peripheral nerve sheath tumors: new patient-derived orthotopic xenografts, cell lines and tumor entities. Mol Oncol 2024;18:895–917.
13. Serra E, Gel B, Fernández-Rodríguez J, Lázaro C. Genomics of peripheral nerve sheath tumors associated with neurofibromatosis type 1. In: Tadini G, Legius E, Brems H, editors. Multidisciplinary approach to neurofibromatosis type 1. Cham: Springer; 2020. p. 117–47.
14. Lee W, Teckie S, Wiesner T, Ran L, Prieto Granada CN, Lin M, et al. PRC2 is recurrently inactivated through EED or SUZ12 loss in malignant peripheral nerve sheath tumors. Nat Genet 2014;46:1227–32.
15. Magallón-Lorenz M, Terribas E, Ortega-Bertran S, Creus-Bachiller E, Fernández M, Requena G, et al. Deep genomic analysis of malignant peripheral nerve sheath tumor cell lines challenges current malignant peripheral nerve sheath tumor diagnosis. iScience 2023;26:106096.
16. Ratner N, Miller SJ. A RASopathy gene commonly mutated in cancer: the neurofibromatosis type 1 tumour suppressor. Nat Rev Cancer 2015;15:290–301.
17. Jessen WJ, Miller SJ, Jousma E, Wu J, Rizvi TA, Brundage ME, et al. MEK inhibition exhibits efficacy in human and mouse neurofibromatosis tumors. J Clin Invest 2013;123:340–7.
18. Serrano M. The INK4a/ARF locus in murine tumorigenesis. Carcinogenesis 2000;21:865–9.
19. Kohlmeyer JL, Lingo JJ, Kaemmer CA, Scherer A, Warrier A, Voigt E, et al. CDK4/6-MEK inhibition in MPNSTs causes plasma cell infiltration, sensitization to PD-L1 blockade, and tumor regression. Clin Cancer Res 2023;29:3484–97.
20. De Raedt T, Beert E, Pasmant E, Luscan A, Brems H, Ortonne N, et al. PRC2 loss amplifies Ras-driven transcription and confers sensitivity to BRD4-based therapies. Nature 2014;514:247–51.
21. Patel AJ, Liao CP, Chen Z, Liu C, Wang Y, Le LQ. BET bromodomain inhibition triggers apoptosis of NF1-associated malignant peripheral nerve sheath tumors through Bim induction. Cell Rep 2014;6:81–92.
22. Kohlmeyer JL, Kaemmer CA, Pulliam C, Maharjan CK, Samayoa AM, Major HJ, et al. RABL6A is an essential driver of MPNSTs that negatively regulates the RB1 pathway and sensitizes tumor cells to CDK4/6 inhibitors. Clin Cancer Res 2020;26:2997–3011.
23. Fernández-Rodríguez J, Creus-Bachiller E, Zhang X, Martínez-Iniesta M, Ortega-Bertran S, Guha R, et al. A high-throughput screening platform identifies novel combination treatments for malignant peripheral nerve sheath tumors. Mol Cancer Ther 2022;21:1246–58.
24. Frahm S, Mautner VF, Brems H, Legius E, Debiec-Rychter M, Friedrich RE, et al. Genetic and phenotypic characterization of tumor cells derived from malignant peripheral nerve sheath tumors of neurofibromatosis type 1 patients. Neurobiol Dis 2004;16:85–91.
25. Perrin GQ, Li H, Fishbein L, Thomson SA, Hwang MS, Scarborough MT, et al. An orthotopic xenograft model of intraneural NF1 MPNST suggests a potential association between steroid hormones and tumor cell proliferation. Lab Invest 2007;87:1092–102.
26. Fletcher JA, Kozakewich HP, Hoffer FA, Lage JM, Weidner N, Tepper R, et al. Diagnostic relevance of clonal cytogenetic aberrations in malignant soft-tissue tumors. N Engl J Med 1991;324:436–42.
27. Legius E, Dierick H, Wu R, Hall BK, Marynen P, Cassiman JJ, et al. TP53 mutations are frequent in malignant NF1 tumors. Genes Chromosomes Cancer 1994;10:250–5.
28. Imaizumi S, Motoyama T, Ogose A, Hotta T, Takahashi HE. Characterization and chemosensitivity of two human malignant peripheral nerve sheath tumour cell lines derived from a patient with neurofibromatosis type 1. Virchows Arch 1998;433:435–41.
29. Inglese J, Auld DS, Jadhav A, Johnson RL, Simeonov A, Yasgar A, et al. Quantitative high-throughput screening: a titration-based approach that efficiently identifies biological activities in large chemical libraries. Proc Natl Acad Sci U S A 2006;103:11473–8.
30. Wang Y, Jadhav A, Southal N, Huang R, Nguyen DT. A grid algorithm for high throughput fitting of dose-response curve data. Curr Chem Genomics 2010;4:57–66.
31. Mathews Griner LA, Guha R, Shinn P, Young RM, Keller JM, Liu D, et al. High-throughput combinatorial screening identifies drugs that cooperate with ibrutinib to kill activated B-cell-like diffuse large B-cell lymphoma cells. Proc Natl Acad Sci U S A 2014;111:2349–54.
32. Chou TC. Drug combination studies and their synergy quantification using the Chou-Talalay method. Cancer Res 2010;70:440–6.
33. Patro R, Duggal G, Love MI, Irizarry RA, Kingsford C. Salmon provides fast and bias-aware quantification of transcript expression. Nat Methods 2017;14:417–19.
34. Soneson C, Love MI, Robinson MD. Differential analyses for RNA-seq: transcript-level estimates improve gene-level inferences. F1000Res 2015;4:1521.
35. Love MI, Huber W, Anders S. Moderated estimation of fold change and dispersion for RNA-seq data with DESeq2. Genome Biol 2014;15:550.
36. Zhu A, Ibrahim JG, Love MI. Heavy-tailed prior distributions for sequence count data: removing the noise and preserving large differences. Bioinformatics 2018;35:2084–92.
37. Koelsche C, Schrimpf D, Stichel D, Sill M, Sahm F, Reuss DE, et al. Sarcoma classification by DNA methylation profiling. Nat Commun 2021;12:498.
38. Southall NT, Jadhav A, Huang R, Nguyen T, Wang Y. Enabling the large scale analysis of quantitative high throughput screening data. In: Handbook of drug screening. 2nd ed. Boca Raton (FL): CRC Press; 2009.
39. Halilovic E, She QB, Ye Q, Pagliarini R, Sellers WR, Solit DB, et al. PIK3CA mutation uncouples tumor growth and cyclin D1 regulation from MEK/ERK and mutant KRAS signaling. Cancer Res 2010;70:6804–14.
40. Kim MJ, Lee SJ, Ryu JH, Kim SH, Kwon IC, Roberts TM. Combination of KRAS gene silencing and PI3K inhibition for ovarian cancer treatment. J Control Release 2020;318:98–108.
41. Dang F, Nie L, Zhou J, Shimizu K, Chu C, Wu Z, et al. Inhibition of CK1ε potentiates the therapeutic efficacy of CDK4/6 inhibitor in breast cancer. Nat Commun 2021;12:5386.
42. Guo L, Li J, Zeng H, Guzman AG, Li T, Lee M, et al. A combination strategy targeting enhancer plasticity exerts synergistic lethality against BETi-resistant leukemia cells. Nat Commun 2020;11:740.
43. Gallagher SJ, Mijatov B, Gunatilake D, Tiffen JC, Gowrishankar K, Jin L, et al. The epigenetic regulator I-BET151 induces BIM-dependent apoptosis and cell cycle arrest of human melanoma cells. J Invest Dermatol 2014;134:2795–805.
44. De Raedt T, Brems H, Wolkenstein P, Vidaud D, Pilotti S, Perrone F, et al. Elevated risk for MPNST in NF1 microdeletion patients. Am J Hum Genet 2003;72:1288–92.
45. Fernández-Rodríguez J, Morales La Madrid A, Gel B, Heredia AC, Salvador H, Martínez-Iniesta M, et al. Use of patient derived orthotopic xenograft models for real-time therapy guidance in a pediatric sporadic malignant peripheral nerve sheath tumor. Ther Adv Med Oncol 2020;12:1758835920929579.
46. Gu Y, Wang W, Li Y, Li H, Guo Z, Wei C, et al. Preclinical assessment of MEK inhibitors for malignant peripheral nerve sheath tumors reveals differences in efficacy and adaptive response. Front Oncol 2022;12:903177.
47. Schulte A, Ewald F, Spyra M, Smit DJ, Jiang W, Salamon J, et al. Combined targeting of AKT and mTOR inhibits proliferation of human NF1-associated malignant peripheral nerve sheath tumour cells in vitro but not in a xenograft mouse model in vivo. Int J Mol Sci 2020;21:1548.
48. Ho WW, Pittet MJ, Fukumura D, Jain RK. The local microenvironment matters in preclinical basic and translational studies of cancer immunology and immunotherapy. Cancer Cell 2022;40:701–2.